Dual Frequency and Dual Circular Polarization Microstrip Nonresonant Array Pin-Fed From a Radial Line

Reuven Shavit, *Senior Member, IEEE*, Lev Pazin, Yaniv Israeli, Michael Sigalov, and Yehuda Leviatan, *Fellow, IEEE*

***Abstract*—A new type of a dual frequency and dual circular polarization multilayer microstrip nonresonant antenna array for satellite communication is presented. The microstrip radiating elements in the array are arranged in concentric circles and fed through pins embedded in a radial line. The radial line is excited through a probe at its center. The microstrip array exhibits a dual frequency band of operation, low side-lobes in the radiation pattern, and high radiation efficiency (more than 65%) for both polarizations. The microstrip element has been designed using commercial software based on the method of finite integral time domain algorithm, and the feed network has been designed by a theoretical analysis. A prototype of the array has been built and tested. The agreement between the measured and numerical results is satisfactory.**

***Index Terms*—Circular polarization, dual frequency, nonresonant microstrip antenna, radial line.**

I. Introduction

The rapid growth of satellite communication has stimulated intensive research concerning medium and high gain planar antennas. Microstrip nonresonant antennas are considered as an obvious choice for such an application due to their low cost, low weight and low profile. However, large microstrip antennas for mid and high gain applications encounter a major deficiency in their performance, due to their high loss experienced in the feed network. These losses reduce the achievable radiation efficiency to less than 40%. A possible solution to this problem is to replace the standard microstrip feed network with a radial line (radial waveguide) feed network. A radial line feed network is subject to much lower losses. Hence, it is an attractive alternative. This type of network was first conceptualized and built by Goebels and Kelly [1] to feed a flat antenna with annular slots as radiators, also called radial line slot antenna (RLSA). A derivative from RLSA concept was studied by Carver [2] and Nakano [3], in which the radiating elements in the array are helices fed from a radial line through small wire pins to obtain circular polarization. The radial line was excited at its center by a probe and the helices were distributed circularly on the top surface of the radial line on concentric circles. In 1991, Haneishi *et al.* [4] replaced the helices with circular polarized microstrip elements to obtain a high efficiency (90%) antenna in Ku band. These elements were used also by Yamamoto *et al.* [5] to design a circular array antenna with shaped beam. In the circular polarization antennas described in [2]–[5], the arrays are nonresonant and uniformly excited. Hence, the outer circle of radiating elements in these arrays is strongly coupled to the waveguide and serves also as an effective termination (load of the waveguide). Other types of the radial line planar microstrip array antennas are described in [6], [7].

In this paper, a new type *Ku* band, dual frequency and dual circular polarization multilayer microstrip array antenna with low side-lobes fed from a radial line through wire pins is presented. The motivation is the design of a two-way terminal antenna for low earth orbit (LEO) satellite communication from a mobile platform. The radiating element is composed from two stacked circular patches fed by a single feeding pin. The circular polarization is achieved for each circular patch by introducing two indents as described in [8]. The uniqueness of the proposed element is that it enables to control independently the radiated phase of each of the patches by turning the two patches around their common feeding point. The computation of the radiation parameters of the radiating element was conducted using the *MWS* commercial software from *CST*, which is based on a finite integral time domain (FITD) algorithm. The radiating elements are distributed on concentric circles and the radial line is fed through a wire probe at its center. The lengths and coupling to the wire pins inserted in the radial line have been determined through an analytical procedure outlined in [9], [10]. A prototype of an array with 8 rings operating in two frequency ranges 11.7–12.2 GHz (low frequency band) with right hand circular polarization (RHCP) and 14–14.5 GHz (high frequency band) with left hand circular polarization (LHCP) has been built and tested. The agreement between the computed and the test results is satisfactory.

II. The Radiating Element

The basic structure of the proposed element operating in two *Ku* frequency bands and two orthogonal circular polarizations is shown in Fig. 1. Two stacked circular patches are fed in tandem by a single pin. Each patch is coupled eccentrically to the feeding pin through an annular gap [11], [12]. This unique type of feeding is necessary in order to introduce a capacitive effect to counterbalance the inductive effect of the feeding pin. The feeding pin is top loaded with a little circular pad as an

Manuscript received February 14, 2005; revised August 21, 2005. This project was supported by ISIS consortium, Trade and Industry Ministry, Israel.
R. Shavit and M. Sigalov are with the Department of Electrical and Computer Engineering, Ben-Gurion University of the Negev, Beer Sheva 84105, Israel.
Y. Israeli is with the Antenna Department, Elta Systems Group Ltd., Ashdod 77102, Israel.
L. Pazin and Y. Leviatan are with the Department of Electrical Engineering, Technion – Israel Institute of Technology, Haifa 32000, Israel.
Digital Object Identifier 10.1109/TAP.2005.859911

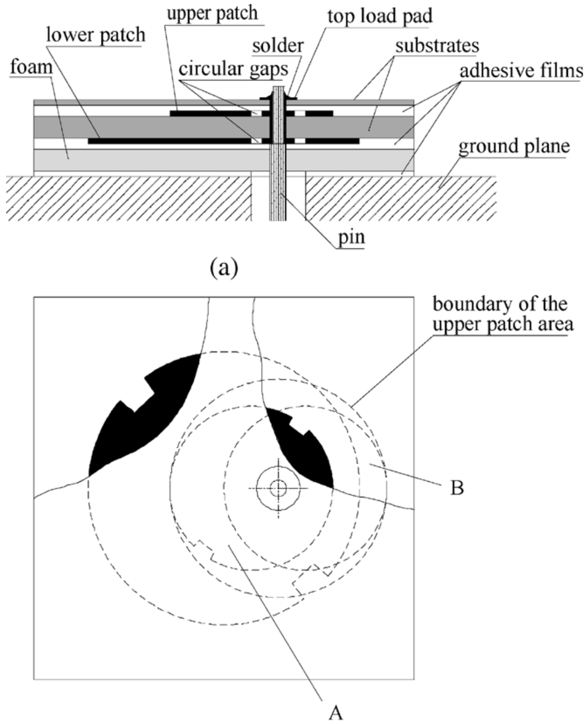

Fig. 1. Geometry of the dual frequency, dual circular polarization microstrip antenna: (a) cross section and (b) top view.

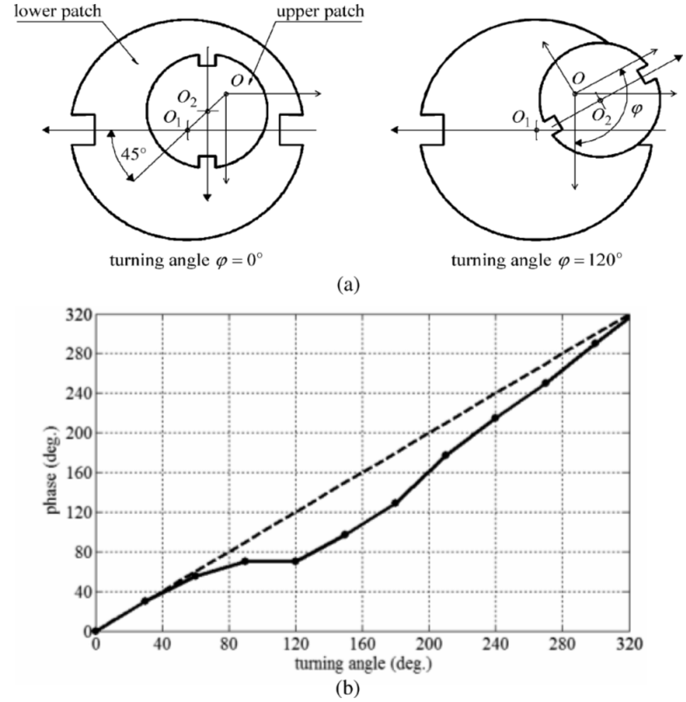

Fig. 2. Effect of the upper patch turning on the electrical phase of the radiated field: (a) lower and upper patch layouts for turning angles $\varphi = 0°$ (to the left) and $\varphi = 120°$ (to the right) and (b) dependence of the electrical phase on the turning angle of the upper patch at 14.25 GHz.

additional matching element. The upper patch "ground plane" is the lower patch. To ensure a large enough "ground plane" for the upper patch in all of its turning angular positions [for example, in positions A and B shown in Fig. 1(b)], the diameter of the upper patch (operating in the upper frequency band) must be considerably less than that of the lower patch (operating in the lower frequency band). This may be achieved by choosing the relative permittivity ε_r of the substrate between the lower patch and the ground plane to be close to unity, and, on contrary, by choice of considerably greater relative permittivity of the substrate between the two patches.

In the design of the proposed element the lowest layer is Rohacell foam with electrical properties $\varepsilon_r = 1.067$, $\tan\delta = 0.0041$ and thickness 0.761 mm. The substrate between the two patches is Rogers RO3006 with electrical properties $\varepsilon_r = 6.15$, $\tan\delta = 0.002$ and thickness 0.64 mm. To reduce mutual coupling among the elements in the array through surface waves coupling, this layer was truncated to a square 12 mm $\times$ 12 mm as shown in Fig. 1. The truncation has a minimal effect on the radiation characteristics of the element. The top pad is printed on the Rogers substrate RO4350 with electrical properties $\varepsilon_r = 3.48$, $\tan\delta = 0.001$ and thickness 0.1 mm.

A parametric study to optimize the element performance was conducted. For the operating frequencies 11.95 GHz (RHCP, lower patch) and 14.25 GHz (LHCP, upper patch), the patch diameters found are 9.14 and 4.24 mm, respectively, and the diameters of the annular gaps are 0.9 mm (inner) and 1.3 mm (outer). The eccentricity of the feeding pin position is chosen by [11] as 1.75 mm for the lower patch and 0.9 mm for the upper patch, to match the radiation element 50 Ohm input impedance of a simple, nonstacked circular patch. As a result, in the considered stacked element, the values of the patch turning angles vary from circle to circle and correspondingly its dimensions, spacing between adjacent elements, mutual coupling and input impedances are changed. The corresponding optimum pad diameter is 1.3 mm. The diameter of the feeding pin is equal to 0.3 mm and the diameter of the pin together with the soldered metalized layer in the substrate package is equal to 0.7 mm. The entire multilayer structure is bonded with adhesive films. The choice of the films has been made based on practical considerations and available adhesive films with electrical properties as close as possible to the corresponding substrate. The adhesive film used to bond the RO4350 substrate to the RO3006 substrate is of thickness 0.1 mm and electrical properties $\varepsilon_r = 3.17$, $\tan\delta = 0.005$, while on both sides of the foam the adhesive films used are of thickness 0.03 mm and electrical properties $\varepsilon_r = 5$, $\tan\delta = 0.005$. The indent dimensions in the circular patches to generate circular polarization [8] are 0.84 mm $\times$ 0.42 mm for the upper patch and 1.6 mm $\times$ 0.8 mm for the lower patch.

The dependence of the radiated electrical field phase on the physical turning angle of the lower patch around the feeding point was tested and found to be linear as expected. To investigate the dependence of the radiated electrical phase variation with the upper patch turning, ten more element prototypes with the upper patch turned around the feeding point (lower patch remaining fixed) in steps of 30° have been fabricated and measured. Fig. 2 shows the effect of the upper patch turning. In Fig. 2(a) one can observe lower and upper patch layouts for counter-clockwise (CCW) turning angles $\varphi = 0°$ (to the left) and $\varphi = 120°$ (to the right). Here, O designates the location of the feeding pin, and O_1 and O_2 denote, respectively, the centers of the lower and upper patches. Fig. 2(b) shows the dependence of the measured radiated electrical field phase at 14.25

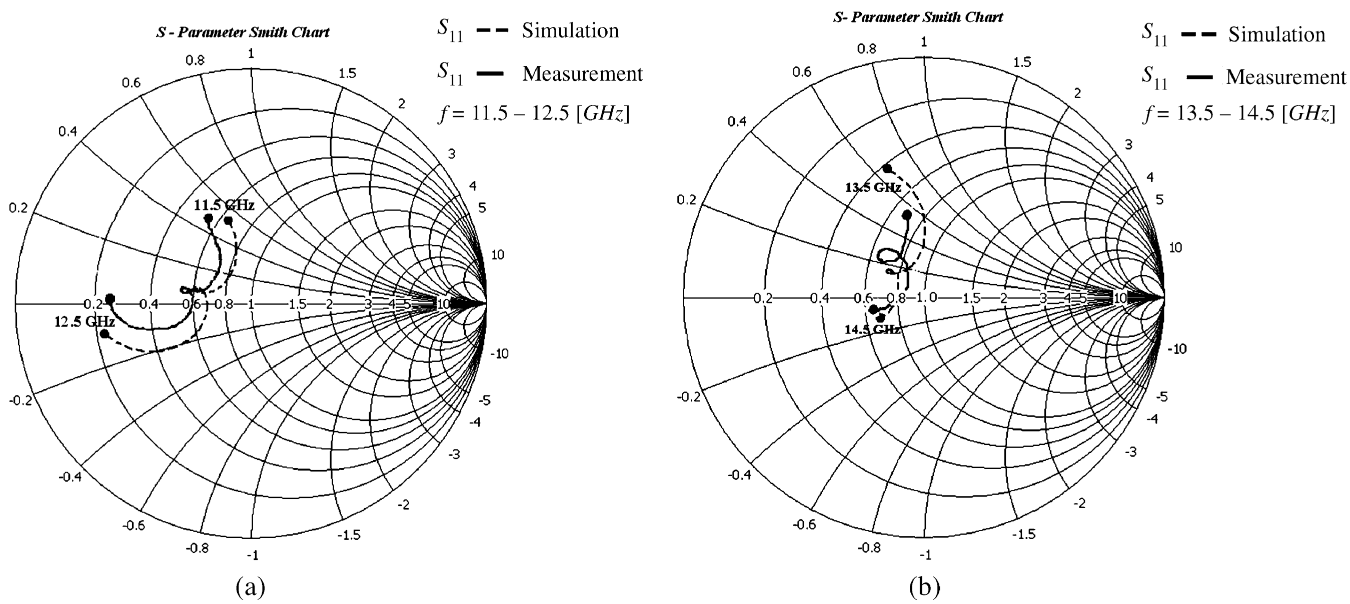

Fig. 3. Radiating element typical input impedance: (a) low frequency band and (b) high frequency band.

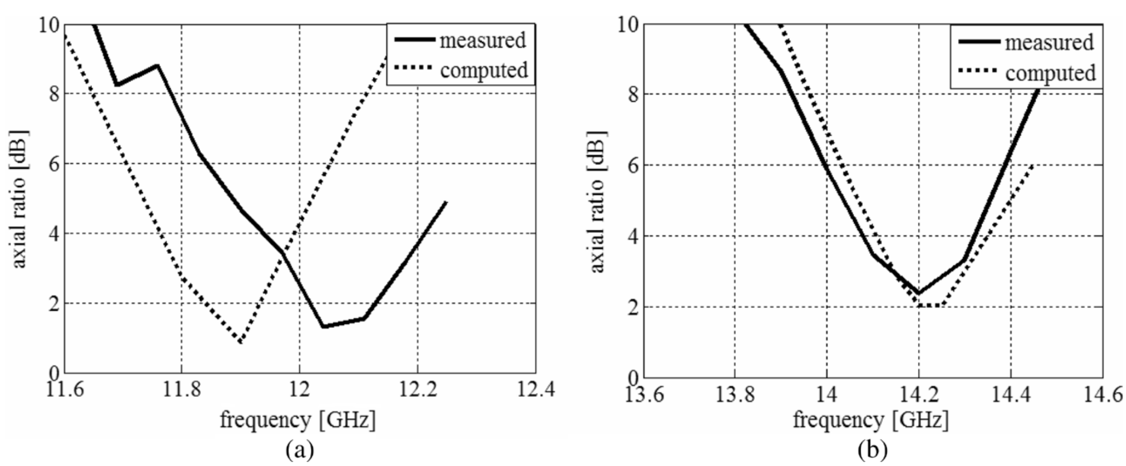

Fig. 4. Radiating element axial ratio versus frequency: (a) low frequency band and (b) high frequency band.

GHz on the turning angle of the upper patch around the feeding point with the lower patch fixed. In a perfect scenario, it is expected that a linear dependence would exist between the phase and the turning angle. As one can notice, the dependence of the measured phase is not perfectly linear due to the inherent asymmetric nature of the structure (the upper patch vis-à-vis the lower patch). This phase variation has been taken in consideration in the array design.

Fig. 3 shows the typical computed and measured input impedance of the stand-alone stacked radiating element. One can observe that the calculated and measured results are in satisfactory agreement. In the feed network design, we used measured values for the input impedances of the radiating elements in each circle. Fig. 4 shows the element axial ratio dependence on frequency. It can be noticed that the measured radiating element axial ratio is 1.4 dB at 12.05 GHz and 2.3 dB at 14.2 GHz. In the high frequency band the agreement between measured and computed values is good. A slight shift can be noticed in the minimum axial ratio location in the lower frequency band, with 12.05 GHz measured value and 11.9 GHz computed value. This shift can be attributed to the multilayer element fabrication process in which some particles of the adhesive film penetrates into the Rohacell foam and changes its electrical properties.

III. Feed Network Design

A picture of the antenna prototype fabricated and its feed network are shown in Fig. 5. The array elements are truncated to a square shape 12 mm $\times$ 12 mm. The truncated element structure contains the two circular patches shown in Fig. 1. The height of the radial line is $S_w = 7.5$ mm, close to quarter-wavelength. A traveling cylindrical TEM mode is generated by the central feeding probe and is propagating along the radial line as a traveling wave weakly coupled to the wire pins of the radiating elements. To avoid reflection from the radial line rim, the residual, nonradiated power (22% at 11.95 GHz and 8% at 14.25 GHz) is absorbed in a matched termination load. The termination load is a one-wavelength wide strip of dielectric flexible absorbing material ARC-LS-10 211 cut in a saw-tooth pattern [termination

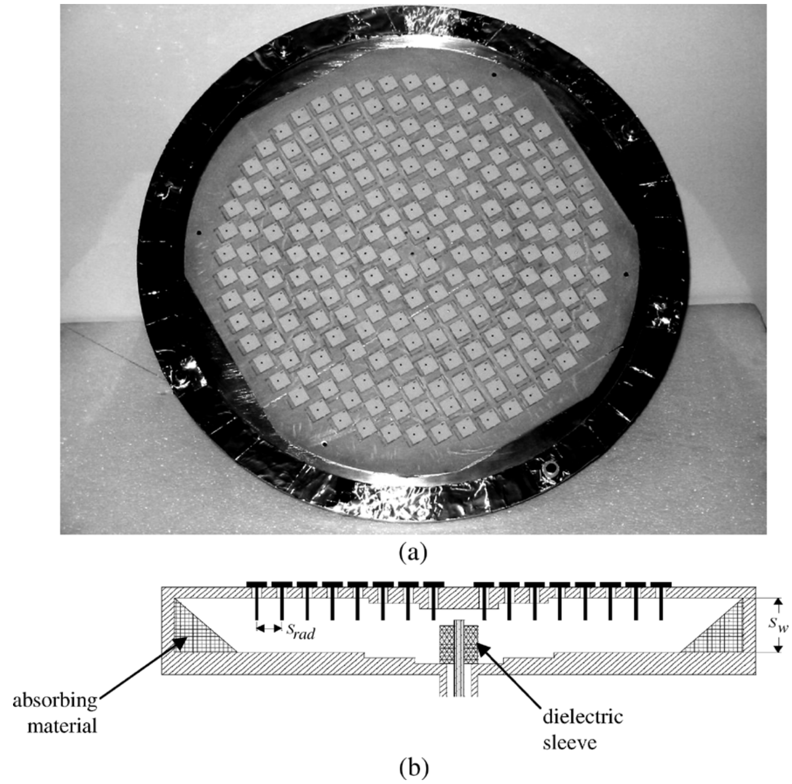

Fig. 5. Microstrip antenna array: (a) top view picture of the prototype and (b) schematic cross section of the feed network.

load is shown schematically in Fig. 5(b)]. To avoid the grating lobes in the radiation pattern, the feeding wire pins of the radiating elements are distributed on concentric circles with radial spacing $S_{\rm rad} = 17.5$ mm (0.7λ at 12 GHz and 0.83λ at 14.2 GHz). To obtain a uniform element distribution on the aperture $(S_{\rm cir} \cong S_{\rm rad})$, it can be shown by [4], the optimal number of radiating elements on each circle N_i should satisfy the condition $N_i = 6i\ (i = 1, 2, \ldots M)$. For practical reasons, the number of circles in this project was selected to be $M = 8$ (total number of elements in the array is 216). The spacing between adjacent pins on each circle is $S_{\rm cir} = 18.3$ mm (0.73λ at 12 GHz and 0.86λ at 14.2 GHz). To improve the antenna input matching over the entire frequency band, the central probe was wrapped with a dielectric sleeve as shown in Fig. 5(b).

Initial uniform phase distribution on the array aperture (neglecting external mutual coupling between radiating elements) can be achieved only for one frequency in each frequency range. This feature is accomplished by turning the upper and lower radiating patch elements independently to offset the variation in the electrical phase delay between adjacent circles in the radial line. The turning angles have been calculated by [9] for the central frequencies of each frequency band.

The crucial part of the design scheme is the determination of the pin lengths $l_{\rm i}$ required to achieve the desired excitation coefficients a_i. To obtain a low side-lobe level in the radiation patterns, an initial bell-shaped amplitude distribution (BSAD) with a taper parameter of $p = 0.7$ has been chosen [9]. The excitation coefficients a_i in this case are given by

$$a_i = 1 - 0.35\left[1 - \cos\left(\frac{\pi i}{M}\right)\right] \tag{1}$$

and presented for $M = 8$ in Table I. The required coupling coefficient, which determines the power delivered by the feed system to the radiating elements, is given in decibels by

$$\mathrm{C}'_{0i} = 10\log\frac{a_i^2}{\sum\limits_{m=i}^{M}(a_m^2 N_m) + q a_M^2 N_M} \tag{2}$$

where q is a termination parameter (a ratio between the power absorbed in the termination load and the total power radiated by all elements of the outer circle [9]). Calculated results of C'_{0i}, for $q = 3$, are presented in Table I. As shown in [10], this coupling coefficient can also be written in terms of the feed network parameters as

$$C_{0i} = 10\log\frac{1.5\left[\tan^2\left(\frac{\pi l_i}{\lambda}\right)\right] R_{{\rm L}i}}{i\left(\frac{S_{\rm rad}}{\lambda}\right)\left(\frac{S_{\rm w}}{\lambda}\right)|Z_i|^2} \tag{3}$$

where $R_{{\rm L}i}$ is the radiating element input resistance, and Z_i is the input impedance of the loaded pin in the array [10]. Now, requiring that C'_{0i} be equal to C'_{0i}, we can derive the pin length $l_{\rm i}$ needed to attain the desired array amplitude distribution.

This procedure takes in consideration the internal mutual coupling among the pins, the loading of the all radiating elements, the waveguide termination, and the transforming properties of the coaxial channels in the radial waveguide cover. Based on the computed coupling coefficients, the required pin lengths for all circles in the array were determined and averaged (see Table I).

One can observe that for the initial BSAD, the variation in the calculated wire pin length is negligible for some circles of the array. This result triggered the idea to divide the radial line

TABLE I
INITIAL VALUES AND FINAL CALCULATED RESULTS OF THE PIN LENGTH AND AVERAGE AMPLITUDE DISTRIBUTIONS ON THE ANTENNA FEED NETWORK

8	7	6	5	4	3	2	1		Circle number, i
0.31	0.34	0.41	0.53	0.67	0.81	0.92	1		Initial relative amplitude, a_i (for BSAD with p=0.7)
-22.8	-23.1	-22.3	-21.3	-20.3	-19.7	-19.2	-18.8		Required coupling coefficients, C'_{0i} (dB)
5.5	5.0	4.1	5.0	3.8	4.4	3.8	3.4	11.95 GHz	Required pin length, l_i (mm)
5.2	3.6	4.1	3.8	3.7	3.2	3.6	2.6	14.25 GHz	
5.3	4.3	4.1	4.4	3.8	3.8	3.7	3.0		Average pin length, $l_{i,\mathrm{av}}$ (mm)
4.3	4.3	4.3	4.3	4.3	3.8	3.8	3.3		Final pin length, l_i (mm)
-25.0	-25.2	-21.3	-23.6	-18.2	-22.0	-19.8	-19.1	11.95 GHz	Final coupling coefficients, C_{0i} (dB)
-24.6	-20.3	-21.4	-19.6	-18.4	-17.6	-18.6	-16.0	14.25 GHz	
0.26	0.27	0.49	0.40	0.94	0.64	0.89	1	11.95 GHz	Final relative amplitude, a_i
0.12	0.24	0.24	0.37	0.53	0.70	0.68	1	14.25 GHz	

in several sections, such that in each section the *coupling* pin lengths l_1 will be kept constant in spite of some distortion of the initial amplitude distribution. Furthermore, to improve the accuracy of the fabrication process, it was realized that it would be more beneficial if the tips of all pins will end at the same z position. Finally, the radial line was manufactured from three sections with compensated jump discontinuities at the interface between adjacent sections as shown in Fig. 5(b) (radial line cross section), while the *total* pin lengths (each pin consists of the *coupling* pin length, the segment in the radiating elements, and the segment in the coaxial channel in the radial waveguide cover) are kept constant and equal to 12 mm. The first section consists of the first circle ($l_1 = 3.3$ mm), the second section consists of second and third circles ($l_2 = l_3 = 3.8$ mm) and the third section consists of the rest of circles ($l_4 = \ldots = l_8 = 4.3$ mm). It should be noted that while the calculated values of the pin lengths of the elements on the fourth circle imply that this circle should have been in the second section of the waveguide, it was nevertheless placed in the third section of the waveguide. This arrangement was made to compensate the error made in the other pin lengths and particularly render the aperture amplitude distribution at the higher operating frequency more close to the desired bell-shaped one. Table I also presents the final calculated average coupling coefficients C_{0i} and amplitude distribution with the above pin lengths to obtain the reduced side-lobe level radiation pattern in both frequency bands. Fig. 6 shows graphically the dependence of the calculated pins coupling coefficients on different circles in the array for the final calculated amplitude distribution.

To assess the magnitude of the external mutual coupling between the array elements, an investigation has been launched to determine its value. Fig. 7 shows the mutual coupling value S_{i1} of a typical element on the second circle to its closest neighbors. One can observe, as expected that the highest mutual coupling is obtained from the closest neighbors on the third and first circles. The maximum value of S_{i1} in the low frequency band it is -20 dB, while in the upper frequency band the maximum value it is -18 dB, which corresponds to known results [13]. The external mutual coupling effect on the antenna

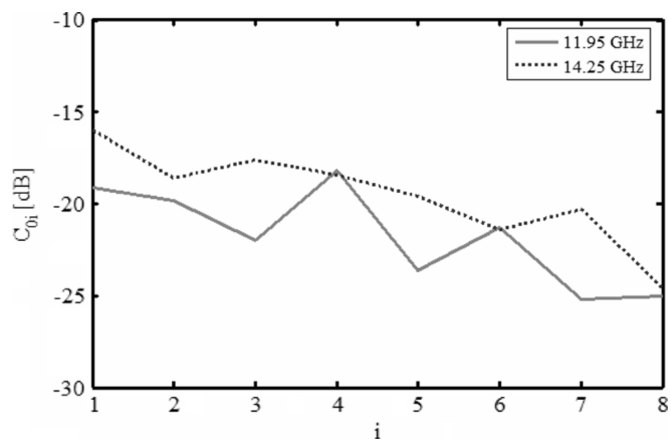

Fig. 6. Coupling coefficient dependence on different circles in the array.

amplitude and phase aperture distributions is random due to the fact that the centers of the radiating elements and their feeding points do not coincide. This introduces also randomness in the distribution of the array elements centers, which reduces the mutual coupling effect. To further reduce the effect of this mutual coupling, it was found experimentally that, for large spacing $S_{\mathrm{rad}} \geq 0.8\lambda$, the pins of the first circle must be shifted by 15° in the azimuthal direction relative to the pins of the second circle (see Fig. 5(a), where the pin positions are shown as dots on the radiating element surfaces). This reduces the frequency-dependent periodic fluctuations of the mutual coupling along the second circle. In the suggested shifted position, all elements of the second circle are equally allocated relative to the pins of the first circle and ensure that all the elements in each of the two circles are equally excited.

IV. EXPERIMENTAL RESULTS

The antenna performance has been tested on a prototype 30 cm in diameter with eight circles 17.5 mm spaced. Figs. 8 and 9 show the measured near-field distribution (amplitude and phase) at the frequencies 11.9 and 14 GHz. One can observe that at 11.9

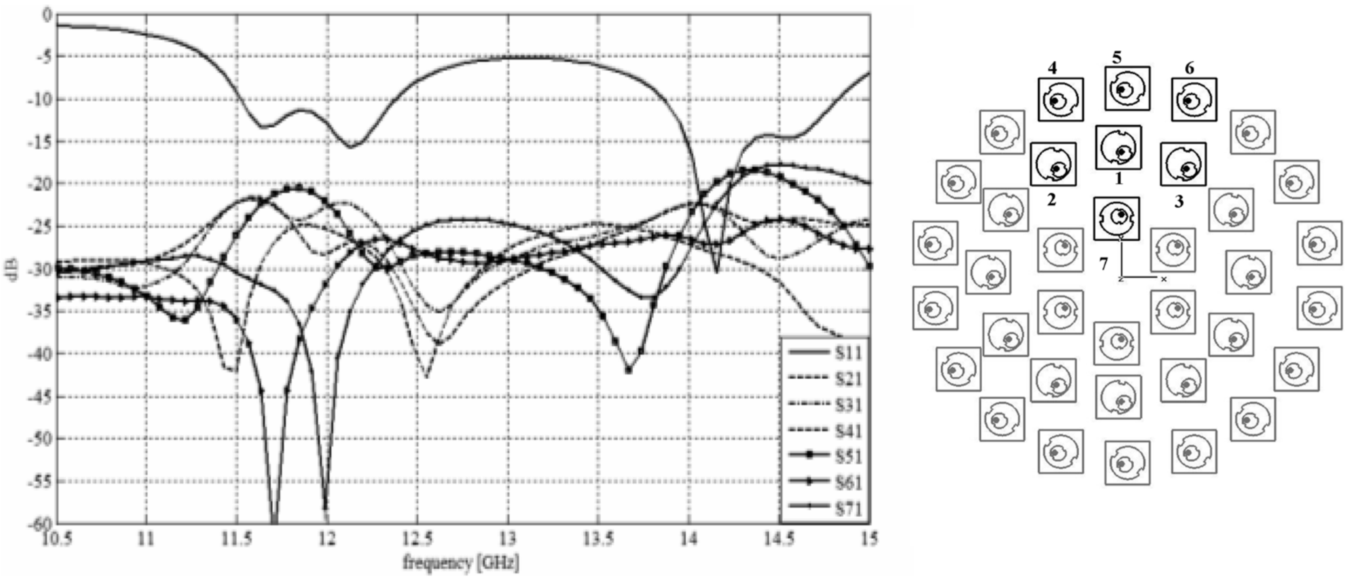

Fig. 7. Return loss and external mutual coupling coefficients for a typical element on the second circle in the array.

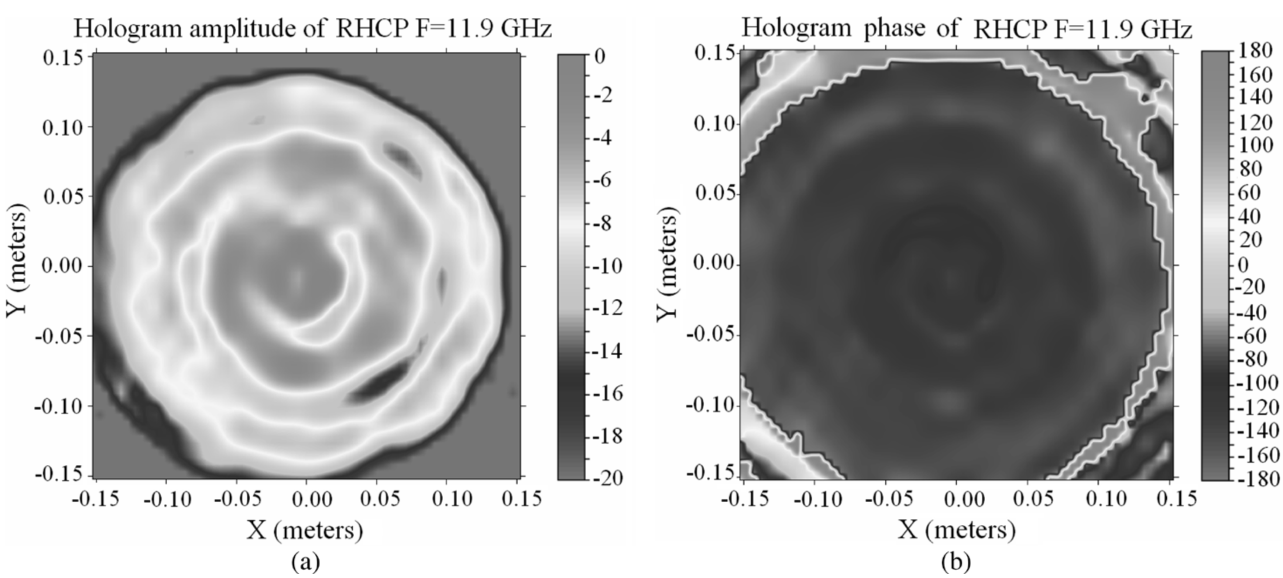

Fig. 8. Array measured near-field distribution at 11.9 GHz: (a) amplitude and (b) phase.

GHz both amplitude and phase distributions exhibit a spiral pattern instead of a ring pattern as expected. Such a distribution can be explained by the nonuniform mutual coupling effect between radiating elements in the array. In the array, the phases of the radiating elements are obtained by locating the pins of the radiating elements on radially equispaced circles and by additional turning of each element around its feeding pin. This element rotation is eccentric and cause nonuniform spacing between elements edges on different circles. Accordingly, the mutual coupling effect between elements on different circles is unequal and perturbs the aperture distribution to a spiral shape instead of a constant circle distribution as desired. At 14 GHz, one can observe a "hexagonal" near-field aperture distribution. Comparison of the measured amplitude distributions in Figs. 8(a) and 9(a) reveals higher tapering at 14 GHz. Results represented in Figs. 8(b) and 9(b) show that the maximum phase deviation in the aperture is approximately $\Delta\phi = \pi/6$. Based on [14], such phase error can lead to some reduction in the gain, though not more than 1.3 dB.

Figs. 10 and 11 show a comparison of computed and measured copol and cross-pol azimuth patterns at 11.9 and 14 GHz, respectively. The computed radiation patterns have been obtained based on the simulated complex fields of the radiating elements on different circles, the final relative amplitude excitations a_{i} described in Table I taking in consideration the position of each pin in the array, and the electrical phase delay between adjacent circles in the radial line. One can observe a satisfactory agreement between the computed and measured radiation patterns. The patterns at both frequencies exhibit a reduced sidelobe level (less than -20 dB). The cross-pol sidelobe level at 11.9 GHz is lower than the sidelobe level at 14 GHz. The main reason for the difference can be attributed to the nonsymmetric nature of the radiating element at the low and high frequency bands as discussed in Section II. Fig. 12 shows the measured return

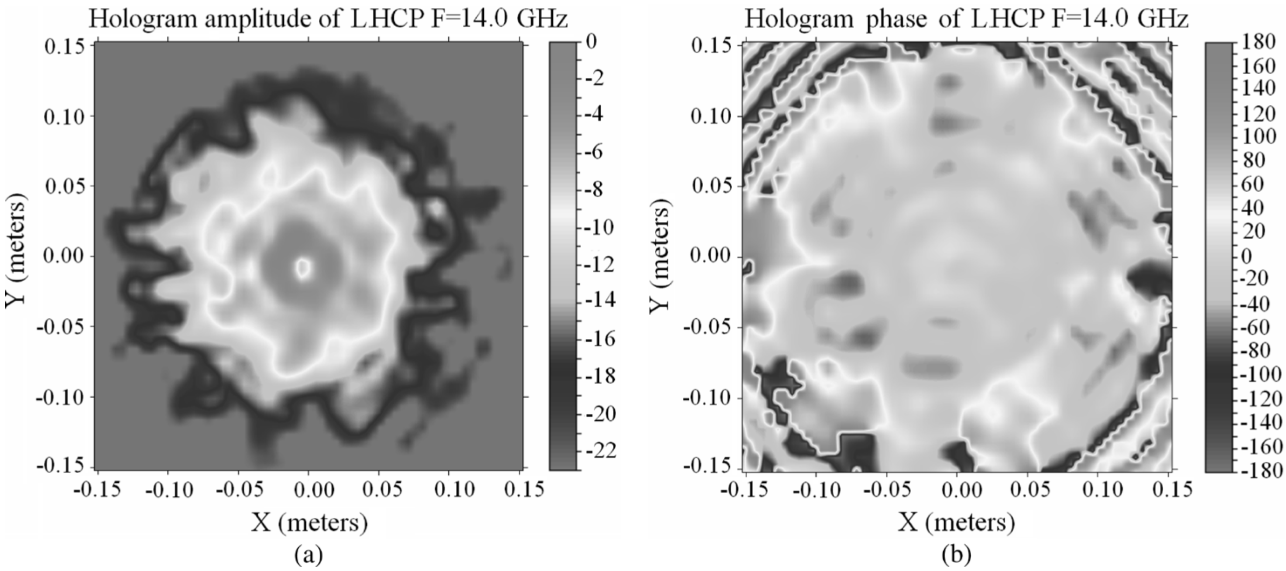

Fig. 9. Array measured near-field distribution at 14 GHz: (a) amplitude and (b) phase.

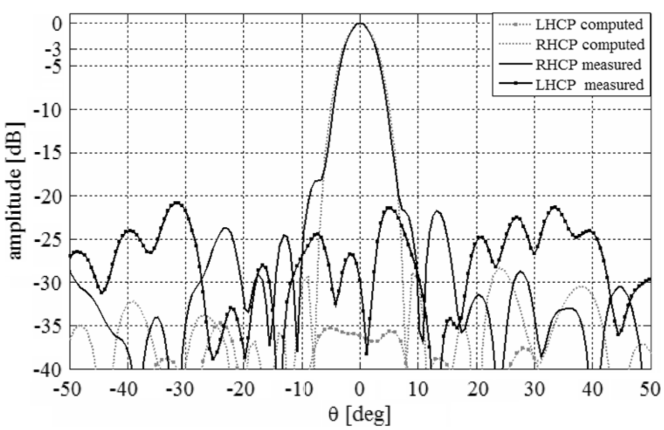

Fig. 10. Azimuth radiation patterns at 11.9 GHz.

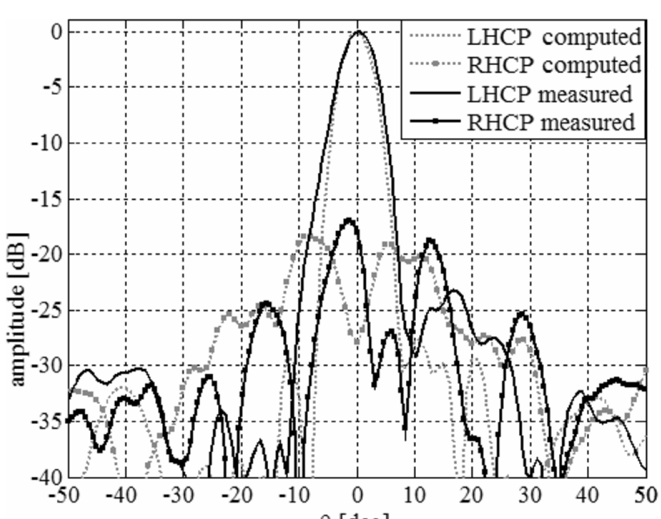

Fig. 11. Azimuth radiation patterns at 14 GHz.

loss of the array in both frequency bands. One can observe a better than -10 dB return loss in both frequency bands, which is characteristics to a nonresonant array and indicates a wide-band good match at the input feed. In the radiating frequency bands the return loss drops to less than -15 dB, due to the radiated energy. Fig. 13 shows a comparison of the computed and measured axial ratio in the low and high frequency bands, respectively. The axial ratio is less than 1 dB in the lower band and less than 4 dB in the higher band. Comparison of these results with the axial ratio dependence on frequency of a single element as displayed in Fig. 4, reveals a much wider bandwidth of the antenna array. This result is due to the averaging effect obtained in the array configuration compared to the performance of a single element. A similar effect was reported in [15] by sequential rotation and phase shifts of the elements in a circularly polarized array antenna.

Fig. 14 shows the computed directivity based on numerical integration of the 3D measured radiation patterns and the measured gain of the antenna in both frequency bands. The efficiency of the antenna (the ratio of gain to directivity) is 65% in the low frequency band and 80% in the high frequency band. A slight shift in the maximum gain frequency location in both frequency bands can be noticed. This shift can be probably attributed to the external mutual coupling between the radiating elements, which has not been considered in this initial design cycle.

V. Conclusion

A new type of a dual frequency and dual circular polarization multilayer microstrip antenna array fed from a radial line was presented. The radiating element is based on a two stacked circular patches fed in tandem by a single pin. The elements in the array are arranged in concentric circles and fed through pins embedded in the radial line. The radial line is fed through a probe at its center. A prototype of the array with 8 rings has been built and tested. The microstrip array with one RHCP/LHCP port exhibits a dual *Ku* frequency band of operation with suppressed side-lobes and high radiation efficiency (more than 65%) for both circular polarizations. The agreement between the measured and numerical results is satisfactory.

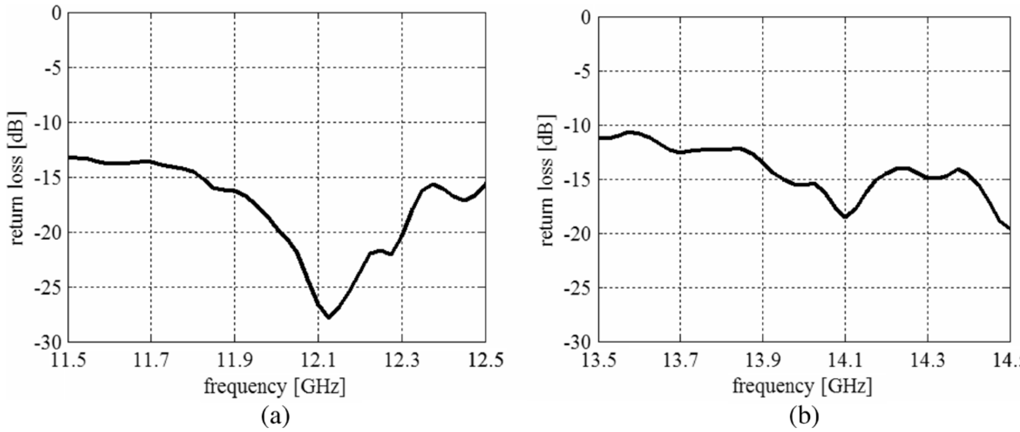

Fig. 12. Measured array return loss versus frequency: (a) low frequency band and (b) high frequency band.

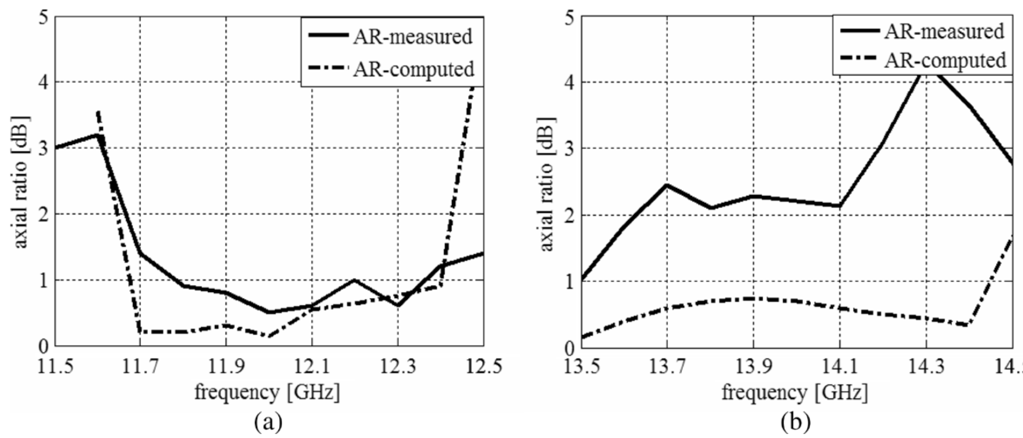

Fig. 13. Axial ratio versus frequency: (a) low frequency band and (b) high frequency band.

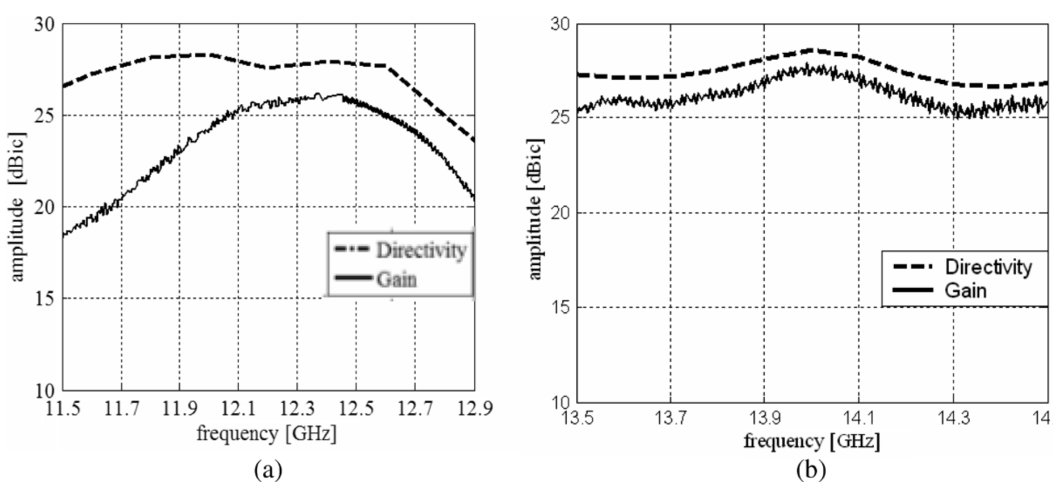

Fig. 14. Gain and directivity versus frequency: (a) low frequency band and (b) high frequency band.

ACKNOWLEDGMENT

The authors would like to express their appreciation to PCB, M. Haemek, Israel and especially to Mr. I. Reef for fabrication of the antenna prototype.

REFERENCES

[1] F. J. Goebels and K. C. Kelly, "Arbitrary polarization from annular slot planar antennas," *IRE Trans. Antennas Propag.*, vol. 4, pp. 342–349, Jul. 1961.

[2] K. R. Carver, "A Cavity-fed concentric ring phased array of helices for use in radio astronomy," Ph.D dissertation, Ohio State Univ., 1967.

[3] H. Nakano, H. Takeda, Y. Kitamura, H. Mimaki, and J. Yamauchi, "Low-profile helical array antenna fed from a radial waveguide," *IEEE Trans. Antennas Propag.*, vol. 3, pp. 279–284, Mar. 1992.

[4] M. Haneishi and S. Saito, "Radiation properties of microstrip array antenna fed by radial line," in *IEEE AP Symp. Dig.*, 1991, pp. 588–591.

[5] N. Yamamoto, S. Saito, S. Morishita, and M. Haneishi, "Radiation properties of shaped beam antenna using radial line microstrip array," in *IEEE AP Symp. Dig.*, 1996, pp. 1924–1927.

[6] H. Miyashita and T. Katagi, "Radial line planar monopulse antenna," *IEEE Trans. Antennas Propag.*, vol. 8, pp. 1158–1165, Aug. 1996.

[7] K. M. Luk, L. K. Au Yeung, and K. F. Lee, “A broadband linearly polarized microstrip antenna array,” in *Proc. Asia-Pacific Microwave Conf., IEICE*, 1998, pp. 1039–1041.
[8] M. Haneishi, T. Nambara, and S. Yoshida, “Study on ellipticity properties of single-feed-type circularly polarized microstrip antennas,” *Electron. Lett.*, vol. 18, pp. 191–193, 1982.
[9] L. Pazin and Y. Leviatan, “Effect of amplitude tapering and frequency-dependent phase errors on radiating characteristics of radial waveguide fed nonresonant array antenna,” *Proc. Inst. Elect. Eng. Microw. Antennas Propag.*, vol. 151, no. 4, pp. 363–369, Aug. 2004.
[10] ——, “Uniform amplitude excitation of radiating elements in array antenna pin-fed from radial waveguide,” *IProc. Inst. Elect. Eng. Microw. Antennas Propag.*, vol. 148, no. 6, pp. 413–417, Dec. 2001.
[11] S. A. Long, L. C. Shen, M. D. Walton, and M. R. Allerding, “Impedance of a circular-disc printed circuit antenna,” *Elect. Lett.*, vol. 14, pp. 684–686, 1978.
[12] P. S. Hall, “Probe compensation in thick microstrip patches,” *Elect. Lett.*, vol. 23, pp. 606–607, 1987.
[13] J. R. James and R. S. Hall, *Handbook of Microstrip Antennas*. Oxford, U.K.: Peter Peregrinus, 1989, vol. 1, p. 252.
[14] D. K. Cheng, “Effect of arbitrary phase errors on gain and beamwidth characteristics of radiation pattern,” *IRE Trans. Antennas Propag.*, vol. AP-3, pp. 145–147, Jul. 1955.
[15] T. Teshirogi, M. Tanaka, and W. Chujo, “Wideband circularly polarized array antenna with sequential rotation and phase shifts of elements,” in *Proc. Int. Symp. Antennas Propag.*, vol. 1, Japan, Aug. 1985, pp. 117–120.

Reuven Shavit (M’82–SM’90) was born in Romania on November 14, 1949. He received the B.S. and M.S. degrees in electrical engineering from the Technion – Israel Institute of Technology, Haifa, Israel, in 1971 and 1977, respectively, and the Ph.D. degree in electrical engineering from the University of California, Los Angeles, in 1982.

From 1971 to 1993, he worked as a Staff Engineer and Antenna Group Leader in the Electronic Research Laboratories of the Israeli Ministry of Defense, Tel Aviv, where he was involved in the design of reflector, microstrip, and slot antenna arrays. He was also a part-time Lecturer at Tel Aviv University, teaching various antenna and electromagnetic courses. From 1988 to 1990, he was associated with ESSCO, Concord, MA, as a Principal Engineer involved in scattering analysis and tuning techniques of high performance ground based radomes. Currently, he is with Ben-Gurion University of the Negev, Beer-Sheva, Israel, as an Associate Professor doing research in microwave components and antennas. His present research interest is in the areas of tuning techniques for radomes and numerical methods for design microstrip, slot and reflector antennas.

Lev Pazin was born in Belarus on May 28, 1932. He received the M.Sc. degree in radio mechanics from the Institute of Fine Mechanics and Optics, Leningrad, U.S.S.R. (now St. Petersburg, Russia), in 1955, and the Ph.D. degree in radio location and radio navigation from the Scientific and Research Institute Mars, Leningrad, U.S.S.R., in 1973.

From 1955 to 1957, he was an Engineer with the Association Ravenstvo. From 1957 to 1998, he was with the Holding Company Leninets in Leningrad, serving as Senior Engineer, Leading Engineer, Senior Scientist, and a Chief of the Laboratory. In 1994, he was awarded an academic title of Senior Research Scientist. Since 2000, he has been with the Department of Electrical Engineering, Technion – Israel Institute of Technology, Haifa, Israel, working as a Research Scientist. He has authored and coauthored 17 inventions and more than 40 journal and conference papers and reports. His main scientific and research interests include array antenna feed networks, near and radiated fields of aperture antennas, and controlled waveguide devices.

Yaniv Israeli was born in Tel-Aviv, Israel in 1974. He received the B.Sc. degree in electrical and computer engineering from Ben-Gurion University of the Negev, Beer-Sheva, Israel, in 2000.

In 2000, he joined the Antenna Department, Elta Systems Group Ltd., Ashdod, Israel, as a Staff Engineer.

Michael Sigalov was born in Erevan, Armenia, in 1972. He received the B.Sc. and M.Sc. degrees in electrical and computer engineering from the Ben-Gurion University of the Negev, Beer-Sheva, Israel, in 2001 and 2005, respectively. Since 2004, he has been working toward the Ph.D. degree at the same university.

His research interests include quantum confinement magnetic-dipolar oscillation in ferrite disks, bianisotropic meta-materials, microwave microscopy and antennas.

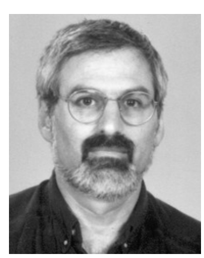

Yehuda Leviatan (S’81–M’81–SM’88–F’98) was born in Jerusalem, Israel, on September 19, 1951. He received the B.Sc. and M.Sc. degrees in electrical engineering from the Technion—Israel Institute of Technology, Haifa, Israel, in 1977 and 1979, respectively, and the Ph.D. degree in electrical engineering from Syracuse University, Syracuse, NY, in 1982.

He spent the 1982/1983 academic year as an Assistant Professor at Syracuse University and subsequently joined the Department of Electrical Engineering at the Technion – Israel Institute of Technology, where at present he is a Professor and the incumbent of the Joseph and Sadie Riesman Chair in Electrical Engineering. During his tenure at the Technion he held short-term visiting positions at Cornell University, the Swiss Federal Institute of Technology (ETH), Zurich, the Catholic University of America, the University d’Aix-Marseilles III, the University of Illinois Urbana-Champaign, the University of Washington, Bell Laboratories, and the University of Michigan. During 1989 to 1991, while on sabbatical leave from the Technion, he was with the Department of Electrical Engineering and Computer Science, The George Washington University, Washington, as a Distinguished Visiting Professor. He is a world-renowned authority in the field of computational electromagnetics. He has published more than 90 journal papers and presented many others at international symposia.

Prof. Leviatan is a Member of Commission B of the International Union of Radio Science (URSI). He was a recipient of the 2001 Henry Taub Prize for Excellence in Research.